Marine and Petroleum Geology 164 (2024) 106847

Contents lists available at ScienceDirect

Marine and Petroleum Geology

journal homepage: www.elsevier.com/locate/marpetgeo

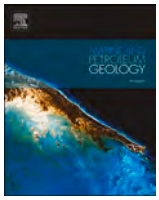

Exploring ophiolitic deposits offshore Scoglio d'Affrica islet (northern Tyrrhenian Sea): A comprehensive geophysical model of the shallow crustal dynamics

Luca Cocchi [a,*], Filippo Muccini [a], Daniele Casalbore [b,c], Francesco Latino Chiocci [b,c], Maria Filomena Loreto [d], Camilla Palmiotto [d], Vincenzo Pascucci [e], Roberta Ivaldi [f], Gilberto Saccorotti [g]

[a] Istituto Nazionale di Geofisica e Vulcanologia, Via di Vigna Murata 605, Rome, Italy
[b] Department of Earth Sciences, Sapienza University of Rome, Piaz.le Aldo Moro 5, Rome, Italy
[c] National Research Council, CNR-IGAG, Piaz.le Aldo Moro 5, Rome, Italy
[d] National Research Council, CNR-ISMAR,Via P. Gobetti, 101, 40129, Bologna, Italy
[e] Department of Architecture, Design and Planning, University of Sassari, Alghero, Italy
[f] Istituto Idrografico della Marina, Ministero della Difesa, Passo dell'Osservatorio 4, Genova, Italy
[g] Istituto Nazionale di Geofisica e Vulcanologia, Pisa, Via Cesare Battisti 53, Pisa, Italy

ARTICLE INFO

Keywords:
Northern Tyrrhenian sea
Gas outburst
Ophiolites
Magnetic anomaly
Multichannel seismic
Inverse modelling
Multibeam swath bathymetry

ABSTRACT

The islet of Scoglio d'Affrica (Tuscany Archipelago, northern Tyrrhenian Sea) is an emerging segment of the Elba-Pianosa Ridge. This ridge is a major tectonic-structural high formed by Eocene-Early Miocene clastic succession which separates the Tuscany shelf from the Corsica basin. The distinctive structural setting of the Scoglio d'Affrica region is a result of crustal fragmentation during the extensional tectonic regime of the northern Tyrrhenian Sea. Along the Elba Pianosa Ridge, a complex interplay between Miocene magmatism, active submarine gas emissions and mud volcanism has been observed. Currently, the Scoglio d'Affrica region experiences active mud volcanism, accompanied by diffuse seafloor gas leakages and sporadic violent mud-water mixed eruptions, as exemplified by the most recent event in 2017.

In this study, we present a comprehensive analysis of shipborne magnetic data, swath bathymetry, single and multichannel seismic profiles of Scoglio d'Affrica region focalized to provide a comprehensive geophysical model of shallow crustal dynamics.

Forward and inverse magnetic models reveal the presence of a continuous high magnetic susceptibility body running along a NNW-SSE direction, parallel to the main tectonic lineaments. This high magnetic source is interpreted as an ophiolite/high grade serpentinite deposit embedded in Eocene siliciclastic layers resulting from the disrupting of the Corsica Alpine basement. This deposits are related to sedimentary gravity processes originated from peripheral highs and accumulated in intra-wedge basins subsequently deformed during the Oligocene. Our reconstruction provides previously unknown details about geometry and distribution of shallow ophiolite-like deposits thereby improving the comprehension the intricate structural evolution of Elba-Pianosa Ridge featured by a multiphase tectonic deformation and shallow manifestations of fluid/gas circulation.

1. Introduction

Submarine mud volcanoes represent one of the surficial expressions of fluids and gas migration (mostly a mixing of them) from the inner crustal regions to the seafloor through preferential zones of weakness within sedimentary layers. These geomorphological features have been extensively studied for their significance in hydrocarbon exploration since the early 20th century (Barber et al., 1986; Hedberg, 1980). They are observed across diverse environments, ranging from continental shelves to abyssal plains, with a great concentration at convergent plate boundaries, and particularly in subduction zones and fold-and-thrust belts (Higgins and Saunders, 1974; Henry et al., 1990; Milkov, 2000;

* Corresponding author.
E-mail address: luca.cocchi@ingv.it (L. Cocchi).

https://doi.org/10.1016/j.marpetgeo.2024.106847
Received 19 December 2023; Received in revised form 3 April 2024; Accepted 4 April 2024
Available online 5 April 2024

Kopf, 2002; Bonini, 2012). The estimated number of known and inferred submarine mud volcanoes ranges between 10^3 and 10^5, surpassing the prevalence of comparable subaerial structures (Milkov, 2000). Submarine mud volcanoes manifest as positive relief often (but not necessary) associated with diapirism and the migration of gas intermixed with water-rich sediments. The extrusion of such mixture of fluids, sediments and gas induces the formation of a breccia-like deposits exhibiting a typical cone-shaped structure with a distinctive central vent. Frequently, these features exist in clusters, forming ensembles of cones and craters (Mazzini and Etiope, 2017). Fluid migration within the sedimentary column primarily results from a buoyancy process between an over-pressurized mud layer and the surrounding rocks. The migrating fluids may originate internally, such as the soluble methane (Hedberg, 1974) or from exotic sources like fluids emerging from deep regions which follow stratigraphic horizons and/or major tectonic elements (Brown, 1990). Gas and water seepage from the seafloor can occur through discrete eruptive events, bringing substantial amounts of fine sediments to the surface over periods ranging from a few hours to several years (Zoporowski and Miller, 2009). The gas emitted from the mud volcanoes typically comprises methane with minor concentrations of CO_2, N_2 and trace amounts of He (Milkov et al., 2003; Mazzini and Etiope, 2017; Saroni et al., 2020). Mud volcanism is a characteristic feature of sedimentary basins placed within the accretional wedge of the subduction system, where high deformation rates create a broad distribution of fault systems capable of driving the fluids up-flow. Numerous instances of mud volcanoes have been identified in the Mediterranean Sea, particularly in the Gulf of Cadiz (Mascle et al., 2014; Nuzzo et al., 2019), along the Calabrian accretionary prism (Praeg et al., 2009), in the southerneast Tyrrhenian Sea (i.e. Paola basin; Rovere et al., 2014, 2022) and in the Mediterranean Ridge (Ivanov et al., 1996; Limonov et al., 1996). On land, mud volcanism correlated to compressive tectonic deformation is well documented in the Northern Apennine (Pede-Apennine margin; Bonini, 2007).

Recently a small mud volcano structure was discovered in the northern Tyrrhenian Sea, offshore the Scoglio d'Affrica islet (also named "*Scoglio d'Africa*" or "*Africhella*"), located approximately 20 km west of Montecristo Island (Fig. 1a). In 2017, the area experienced an intense gas burst at the top of this mud volcano that generated a 10-m-height column of mud and water mixture that ascended from the sea surface. This violent episode lasted for a few minutes and gradually diminished in intensity as witnessed by local fishermen. Within a few days after the outburst, remotely operated vehicle (ROV) imagery unveiled a flat crater, approximately 15–20 m in diameter at the summit (about 7.5 m below the sea level) of a large mound. The occurrence of this intense gas-water-mud eruption triggered a series of new geophysical, morphological and geochemical investigations in the study area.

Casalbore et al. (2020) reconstructed the seafloor morphology of the region using very high-resolution multibeam bathymetry and ROV footage, revealing a mud volcano composed of two distinct mounds aligned NNE-SSW. The 2017 eruption occurred atop the southern mound. Recent studies by Spatola et al. (2022) have identified additional potential mud volcanoes and numerous pockmarks in the nearby area.

Here we present an analysis of magnetic and morphologic data acquired a few months after the 2017 eruption, integrated with previous seismic reflection profiles and stratigraphic well sequences. This study identifies, for the first time, a significant tectono-stratigraphic element within the study area, interpreted as serpentinitic/ophiolitic deposits emplaced within the Eocene sedimentary sequence. This rock-ensemble can be related to the disruption of the Alpine Corsica basement, an ancient fragment of the Tethys Ocean that underwent metamorphic and serpentinization processes (Lagabrielle et al., 2015 and references therein).

The serpentinization process promotes multiple physical-chemical reactions, including the dissolution of inorganic carbon with the formation of CH_4-enriched compounds (Klein et al., 2014). Additionally, the low temperature, fluid-mediate hydration alteration induces a mineralogical replacement of the primary minerals of mantle peridotite, such as Olivine and Pyroxene. Under static and high reduction condition, the alteration of primary 2FeO-rich minerals produces Fe_2O_3 secondary minerals like as Serpentine, Brucite, Magnetite, Talc and Clorites (Toft et al., 1990; Pettke and Bretscher, 2022). The serpentinization of peridotite leads to an increase in the magnetic susceptibility of the hosting rock, which can vary widely (0.001–0.09 SI) as directly correlated to the degree of alteration (Oufi, 2002; Maffione et al., 2014).

The new geophysical model presented in this study quantitatively identifies and reconstructs the depth distribution of ophiolite/high-grade serpentinite deposits along the western flank of Elba-Pianosa

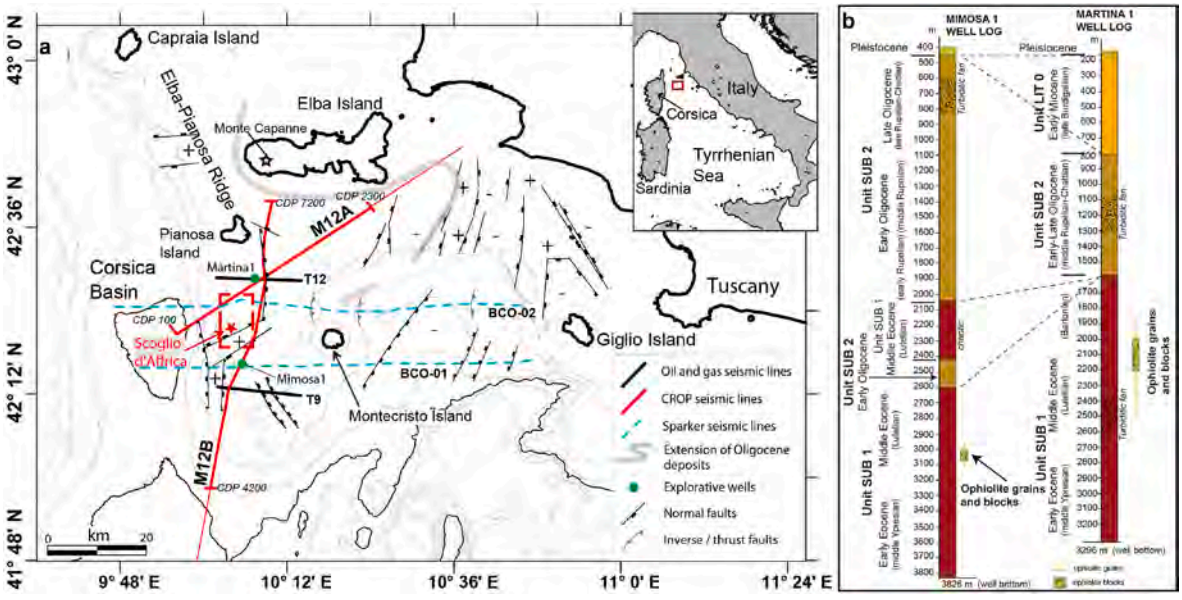

Fig. 1. (**a**) Structural sketch map of Corsica Basin-Tuscan archipelago region (after Cornamusini et al., 2002; Mauffret et al., 1999; Pascucci et al., 1999) with location of the tracks of the seismic lines. Dashed red box indicates the area of the new magnetic and bathymetric surveys. Geographical positions of the Martina-1 and Mimosa-1 explorative wells are from Videpi database (www.videpi.com). (**b**) Stratigraphic sequences of Mimosa-1 and Martina-1 wells simplified from Cornamusini and Pascucci (2014); the well depths are referred to the sea level.

Ridge (EPR, hereafter), postulated to be responsible for the NNW-SSE magnetic anomaly pattern.

2. Geological setting

The Scoglio d'Affrica islet lies along the southern edge of the EPR, a structural element striking roughly in a north-south direction and connecting Elba and Pianosa islands. Positioned between Corsica Island and the Italian peninsula (Fig. 1a), the intricate geologic setting of this tectonic domain is intimately linked to the opening of the Tyrrhenian basin.

The evolution of the northern Tyrrhenian Sea remains a subject of debate in the literature. Most authors suggest that the opening process commenced in the Eocene, coinciding with the closure of the Tethys ocean and the eastward retreat of the west-dipping Adria-Paleo-European subduction system (Bartole, 1995; Jolivet et al., 1998; Cornamusini et al., 2002; Molli, 2008; Carminati and Doglioni, 2012). However, this tectonic scenario is contested by an alternative model proposing an Eocene east-dipping oceanic subduction, followed by slab breakoff and mantle exhumation in the Oligocene (Marroni et al., 2010). Despite variations in the interpretations regarding the onset of basin opening, the first syn-rift deposits are recognized along the Corsica and Sardinia margin, dating back to the Early Miocene (Burdigalian). During this phase, the rollback movement induced an extension of the western sector of the Tyrrhenian area, characterized by a gradual extension rate (1–2 cm/y) and the formation of N–S and NE-SW oriented basins (Faccenna et al., 2001, 1997; Jolivet et al., 1998; Mauffret et al., 1999; Pascucci et al., 1999). Additionally, according to Bonini et al. (2014), the northern Tyrrhenian basin experienced compressional tectonic events also between the Late Miocene and Early Pliocene (approximately 8-3.5 Ma).

The crustal extension and basin formation occurred concurrently with magmatic episodes. Initially, these occurred in the Corsica region with the emplacement of Lamproïte sills at 13.5 Ma, followed by younger volcanic formations along the central (e.g., Montecristo Island at 7.3 and 7.1 Ma) and eastern margins (e.g., Elba Island and Monte Capanne at 8.2/6.2 Ma) (Jolivet et al., 1998; Savelli, 2000; Serri et al., 2001).

The western edge of the Tyrrhenian Sea is characterized by the presence of Corsica-Sardinia massif, a rotated tectonic block of Alpine origin related to the Early Miocene back-arc rifting and opening of the Ligurian-Provençal basin (Gueguen et al., 1998; Speranza et al., 2002). Corsica Island exhibits a complex geological evolution, delineated into two principal structural domains (Molli, 2008): i) the Hercynian sector composed of autochthonous undeformed crystalline-basement rocks and ii) the Alpine region comprising a sequence of metamorphic rocks, ophiolites and flysh (Malavieille et al., 1998; Marroni and Pandolfi, 2003).

The central portion of the northern Tyrrhenian Sea (Fig. 1a) exhibits a distinctive pattern of nearly north-south oriented horst and graben sequences as response to a brittle deformation in a regime of tectonic fragmentation (Bartole, 1995; Pascucci, 2002; Cocchi et al., 2016). One prominent structural high in this area is represented by the EPR, situated between the Corsica basin and the Tuscan Shelf. Its northern sector is characterize by volcanic island of Capraia and the intrusive plutonic rocks occurring at Mt. Capanne (Elba Island) and Montecristo Island. South of Elba Island, the EPR emerges at Pianosa Island, which is mainly formed by Early Miocene (Burdigalian) Late Miocene (Tortonian-Early Messinian) and Pleistocene marine and continental deposits (Bossio et al., 2000). Progressing southward, the EPR crops out at the Scoglio d'Affrica, an uninhabited islet formed by shallow marine Pleistocene calcarenites resting above Triassic-Liassic limestones and the metamorphic basement (Cornamusini et al., 2002; Motteran and Ventura, 2005). The compressive tectonic deformation in this sector is primarily associated with thrust-like kinematics, which is accountable for the observed antiform arrangement of the Eocene-Miocene sedimentary sequence (Buttinelli et al., 2024).

This region underwent extensive exploration by AGIP Spa (Italian Oil & Gas Company) in the 1970s, involving seismic surveys and exploratory drillings. The Mimosa-1 and Martina-1 wells recovered approximately 3380 m and 3127 m of Eocene–Oligocene siliciclastic deposits, respectively (Fig. 1b). Stratigraphic data from Martina-1 reveal the occurrence of coarse gravel-sized clasts comprised of ophiolite rocks, specifically serpentinites, ophiolitic breccias, and minor gabbros. These clasts are widely dispersed within the Eocene sediments, ranging in depths from 2000 m to 2200 m below sea level (b.s.l., hereafter). Within this stratigraphic context, finer-sized serpentinite clasts are prevalent in a broader range of the log, spanning depths from 1850 m to 2500 m, and exhibiting an increase in abundance upward (Cornamusini and Pascucci, 2014).

Additionally, the high abundance of greenish shales and the presence of extraclasts of chlorites observed throughout both sedimentary sequences (see supplementary information in Cornamusini and Pascucci, 2014), can suggest a potential link with the serpentinization process.

Submarine gas exhalations near the Scoglio d'Affrica area have been documented since the early 1960s (Del Bono and Giammarino, 1968; Motteran and Ventura, 2005). Pioneering marine surveys conducted by scuba divers (Barletta et al., 1969) revealed the presence of a network of faults and fractures often associated with gas emissions mainly composed of CH_4 and minor concentrations of N_2, O_2 and CO_2. The origin of these gas seeps remain uncertain and it is still a subject of discussion (e.g. Meister et al., 2018). More recently, Saroni et al. (2020) conducted a geochemical study of the gas emissions around Scoglio d'Affrica revealing a methane composition of thermogenic origin contrasting with those sampled offshore Elba Island (Scoglio dell'Ogliera, Pomonte site) which exhibit a certain abiotic signature (Sciarra et al., 2019).

3. Data and methods

In July 2017, a new magnetic and bathymetric investigation of the Scoglio d'Affrica offshore region was performed in collaboration with the Italian Navy-Hydrographic Institute (Istituto Idrografico della Marina, IIM) on board the R/V Aretusa. This survey was performed to identify any potential causative sources responsible for the 2017 gas outburst.

3.1. Shipborne magnetic survey

Magnetic data were collected using a SeaSpy Marine Magnetics magnetometer towed about 50 m astern of a hydro-jet survey boat. The vessel was equipped with DGPS positioning (Omnistar-VBS correction) and a QPS Qinsy navigation system. Raw magnetic data, sampled at 1 Hz, were collected using the SeaLink software suite which also ensured a synchronous GPS lay-back correction for the precise positioning of the magnetic sensor at sea.

The magnetic survey was planned taking into account various factors such as water depths, the seafloor morphology and also the magnetic anomaly pattern of the study area from available regional data (i.e. aeromagnetic data, Caratori Tontini et al., 2004). The magnetic investigation was conducted following a set of 20 E-W (average heading N85°) parallel survey lines and 2 orthogonal control tie lines (Fig. 2a). The resulting dataset comprises over 480000 data records collected along 152 linear km.

The total-field magnetic data were processed removing spikes and outliers. Despite the inherently low magnetic signature of the small fiberglass boat, a heading correction was applied to minimize the (very low intensity) magnetic noise generated by the vessel. To account for the time dependence of the Earth's Magnetic field, daily magnetograms from the Duronia geomagnetic observatory in Italy (https://www.intermagnet.org) were utilized. Diurnal correction was applied by subtracting the time-dependent magnetic contribution directly from the raw dataset. Systematic errors arising from variation in velocity, depth

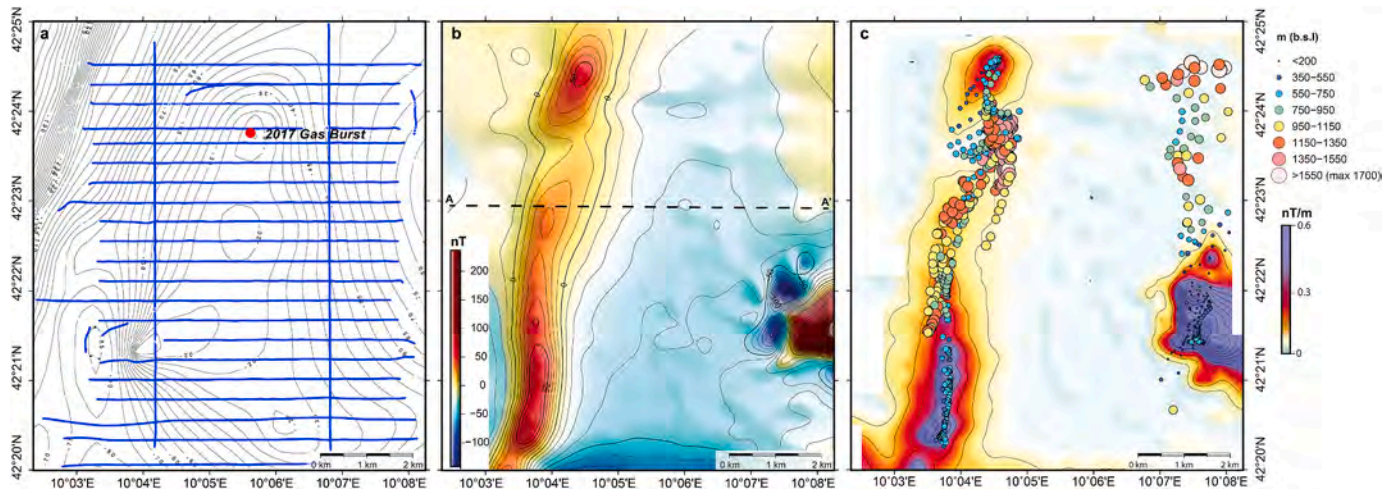

Fig. 2. (**a**) Layout of shipborne magnetic survey of Scoglio d'Affrica area performed in 2017. Red filled point indicates the position (at sea-level) of the gas burst occurred in March 2017. Contour lines represent the isobaths derived from EMODnet DTM 2020 (EMODnet Bathymetry Consortium, 2020). (**b**) Total field magnetic anomaly field acquired during the 2017 survey (panel a). A-A′ black dashed line identifies the track of the magnetic profile used in the forward model (Fig. 8). (**c**) Map of analytic signal derived from magnetic anomaly field. Coloured circles indicate the position of the Euler's solutions; the symbols size is proportional to the depth of the magnetic source.

position of the two-fish and a not perfect navigation of the vessel were assessed through a statistical analysis of the cross points between parallel (E-W) and orthogonal (N–S) survey-lines. The cross-over errors were removed applying a statistical levelling. The magnetic anomaly field (Fig. 2b) was computed by subtracting from the corrected total intensity field the deep contribution of the Earth's magnetic field derived from the IGRF model (Alken et al., 2021). The intrinsic dipolar behaviour of the magnetic anomaly field has been corrected by applying the reduction to the pole (RTP) algorithm (Baranov and Naudy, 1964) (Fig. S1). This transformation involves a FFT-phase shifting using present-day values of inclination (55.2°) and declination (2.6°) of Earth's Magnetic field, as derived from the IGRF model.

A qualitative evaluation of the distribution of magnetic sources was achieved by estimating the 3D analytic signal (Fig. 2c). This mathematical procedure is based on the summation of the horizontal and vertical derivatives of the magnetic anomaly field (total intensity) (Nabighian, 1984). It represents a very useful analytic approach aimed to enhance the edges of the causative sources (or ensembles of sources). In fact, distribution of analytic signal yields a bell-shape curve with maximum amplitude coinciding with the lateral boundaries of the magnetic sources. Starting from the magnetic gradient estimation, we performed a qualitative evaluation of the depth distribution of the causative magnetic bodies employing the Euler's deconvolution techniques (Reid et al., 1990; FitzGerald et al., 2004). This methodology relies on a least-square inversion of the Euler's homogeneity equation applied to the magnetic anomaly data utilizing a specific structural index (SI) (Thompson, 1982). This parameter can vary from 0 to 3 considering the specific geometry of the magnetic sources. In our case, we used SI equal to 1 (tabular, sill and horizontal sequence) as optimal value because it results in a most compact distribution (high clustering) of the solutions.

3.2. Magnetic modelling

The magnetic forward model technique permits a qualitative reconstruct of the geometry and magnetic susceptibility properties of potential causative sources along a cross section. In this study, observed data were sampled from an interpolated grid along the profile A-A' (W-E oriented, Fig. 2b), intersecting the major magnetic features of the Scoglio d'Affrica region.

The forward model computation was carried out using GmSYS tool of Oasis Montaj software suite (Seequent Ltd) based on analytical algorithms (Talwani and Heirtzler, 1964; Won and Bevis, 1987). This approach primarily involves estimating the best fitting between the observed magnetic profile and the synthetic one derived by a distribution of causative bodies with shape and magnetic susceptibility defined by the user. To enhance the interpretation, a 2.5D forward modelling approach was employed, accounting for variations in shape and susceptibility of the different rock blocks both along and across (in symmetric manner) the track profile.

The geologic cross section was constrained using the local stratigraphic data obtained from the Martina-1 well (Fig. 1.b; Cornamusini and Pascucci, 2014). The forward computation was performed using intensity (average value 46212 nT), inclination and declination values of the local geomagnetic field (from IGRF; Alken et al., 2021).

Subsequently, a quantitative interpretation of magnetic anomaly data of the Scoglio d'Affrica region was achieved by using a tridimensional inversion. Data were inverted utilizing a voxel mesh with an upper bound defined by the seafloor morphology and a flat bottom layer placed at depth of 3.0 km. The total magnetic field was sampled at the center of each cell and the target misfit set to be variable for the resulting observation points of the model. The mathematical algorithm combines a Cartesian cut cell (CCC) (Ingram et al., 2003; Ellis and MacLeod, 2013) approach and the Iterative Reweighting Inversion (IRI) focusing (VOXI ™) method to model sharpen contacts. Resulting susceptibility values have been bounded in the range of ±0.1 SI based on the expected magnetic signature of the crustal structures. Several inversions were performed, varying parameters such as the horizontal and vertical gradient weighting factors and the IRI focus value.

The final selected model represents the best solution that aligns the available geological information, exhibiting the lowest difference between the observed and predicted data, i.e. Root Mean Squared (RMS) misfit equal to 1.4 after 32 iterations.

3.3. Bathymetry survey

Multibeam bathymetry survey was performed in 2017 collecting data over an area of 75 km^2, using Kongsberg EM2040 and EM2040C multibeam systems working at a frequency of 300/400 kHz. Vessel positioning was supplied by DGPS FUGRO 9205 GNSS, with Marinestar HP + G2 corrections. Sound velocity profiles were collected using the Valeport MiniSVP probe, while tidal data were downloaded from the ISPRA gauge at Marina di Campo (Elba Island). Bathymetric raw data were processed with CARIS Hips & Sips 9.0.1 using the CUBE algorithm

to provide Digital Elevation Model (DEM) with a cell-size of 0.5 m; the accuracy of bathymetric data is less than 1.22 m and 0.64 m for the horizontal and vertical planes, respectively. DEM was used to derive the slope gradient map and to parameterize the main seafloor geomorphic features through Global Mapper software (Blue Marble Geographics).

3.4. Previous seismic data

The EPR has been largely surveyed by several seismic reflection profiles in the past. This study contributes a novel and detailed stratigraphic analysis of the study area, incorporating and reinterpreting diverse seismic data sources, as depicted in Fig. 1a. The analyzed datasets include:

i) High-resolution seismic profiles. The vintage sparker profiles used in this work (BCO-01 and BCO-02; blue dashed lines in Fig. 1a) are part of the CNR database acquired on board of R/V Bannock during 1970s and 1980s (Fabbri et al., 1981)("*Progetto Finalizzato – Oceanografia e Fondali Marini*"). These profiles were acquired using a 30-kJ seismic source from Teledyne Exploration (Huston, USA), with a shooting interval of 25 m and a record length ranging from 4 to 8 s (TWT). BCO-01 and BCO-02 profiles are part of the digital Sparker DataBank (SDB, CNR) designed to preserve and reuse vintage data (Ferrante et al., 2023). To enhance accessibility and usability, printed seismic lines were initially scanned to produce high-resolution raster images (TIFF), which were then converted into standard georeferenced SEGY profiles using the IMAGE2SEGY tool (Farran, 2008).

ii) Deep crustal multi-channel lines (CROP project). The Scoglio d'Affrica region was explored by two multichannel seismic lines (M12A and M12B; red lines in Fig. 1a) being part of the CROP database (CROsta Profonda; www.crop.cnr.it; Scrocca et al., 2003; Finetti, 2005). These lines were acquired in the early '90s and utilized marine data acquisition techniques involving 4 tuned arrays of 32 airguns and a 4500 m long streamer with 180 channels spaced 25 m apart. The shot interval was 50 m, providing a coverage of 4500%. Stacked M12A and M12B profiles have been post-stack time-migrated using a seismic velocity of 1530 m/s at the seafloor and increasing with depth.

iii) Oil and gas exploration seismic surveys. Agip Spa (now Eni S.p.A) conducted an active exploration of Tuscany basin since 1970, conducting seismic reflection surveys and drilling operations (Mimosa-1 and Martina-1 wells) (Pascucci et al., 1999; Pascucci, 2002). Among all the numerous of seismic lines spanning the northern Tyrrhenian Sea (www.videpi.it), we have selected the T9 and T12 lines (black lines in Fig. 1a) because they partially intersect the Scoglio d'Affrica region. These profiles were acquired using an airgun source, and a streamer equipped by 240 hydrophones; the shot interval ranged from 13 m to 26 m. Data were processed and time-migrated as outlined by Mariani and Prato (1988).

The seismic lines underwent a detailed analysis providing a detailed interpretation of the main sedimentary units spanning from the Eocene to the Plio-Quaternary. This interpretation was conducted using the Kingdom Suite software (IHS Markit). The identification of the several seismic facies (base of Pliocene, of Miocene and of Oligocene or top of Eocene) was constrained by using the Mimosa-1 and Martina-1 stratigraphic sequences. The projection of stratigraphic sequence on the seismic line required a depth conversion using a seismic velocity equal to 3300 m/s.

In addition, a 2D geometrical reconstruction of the seismic horizon associated with the top of Eocene was performed, time-deriving its distribution from sparker (BCO-01) and multichannel seismic lines (M12A-B and T12 lines), and finally creating a 100 m grid cell size map.

4. Results and interpretation

4.1. Morpho-bathymetric data

The study area is located between 3 and 155 m water depths (wd, hereafter), corresponding to the upper part of the EPR (Fig. 3a). The distribution of geomorphic features in the area can be divided into two sectors:

a) the shallow (first 50 m wd) and gently sloping top-of-the-ridge central sector is morphologically characterized by several cone-shaped morphological highs, with diameters of some hundreds of meters and heights of few tens of meters. They generally have a flat summit and steep flanks (Fig. 3b), where lobate-like flows are sometimes recognized. Direct observations through ROV and scuba dives on two of these features have detected diffuse seepage and mud-breccia (Casalbore et al., 2020; Saroni et al., 2020; Ferretti et al., 2021), leading to interpret them as mud volcanoes (MV in Fig. 3a). Particularly, the mud volcano responsible for the 2017 outburst is made of two small coalescence mounds, forming an NNE-SSW elongated ridge. Besides these mud volcanoes, the area is characterized by small patches of irregular seafloor, interpreted as sandy patches that interrupt the continuity of the *Posidonia oceanica* meadows, and by sub-circular or slightly elongated depressions interpreted as pockmarks, with diameters of few tens of meters and negative relief of a few meters (Spatola et al., 2022).

b) The western and eastern ridge flanks are instead characterized by a steeper seafloor, morphologically dominated by a series of steep (on average 15°, locally up to 40°) and linear escarpments, mainly oriented along N–S and NNE-SSW directions. These features are several hundred meters long and a few tens of meters high, sometimes delimiting elongated channels, as for instance observed in the northern part (Ch in Fig. 3a). Along the western flank, a series of sub-circular or irregular morphological highs (MH in Fig. 3a) are present, with a maximum diameter of few hundred meters and maximum relief of ~10 m with respect to the surrounding seafloor. Their top is almost flat and smooth, and aligned along a NNE-SSW direction or forming ridges elongated in the same direction (ridges in Fig. 3a).

4.2. Magnetic data and modelling

The shipborne dataset collected during the 2017 oceanographic cruise represents the unique available, high resolution magnetic set of data of this portion of the northern Tyrrhenian Sea.

The study area shows a low amplitude magnetic anomaly pattern (Fig. 2b) related to the geological background mainly formed by clastic successions having a low-to-null magnetic susceptibility. Anyway, the eastern portion of the survey area shows a very intriguing singularity: a N–S oriented, 10 km-long magnetic anomaly, ranging between −30 and +100 nT. This anomaly is well distributed along the entire survey region and it probably extends also further. East of the structure another high positive magnetic peak ranging about 120–150 nT is present. This magnetic high has a very complex geometry with a clear dipolar shape still observable in the RTP anomaly map (Fig. S1). The positive-negative dipolar distribution seems oriented in E-W/NW-SE direction, which is not parallel to the declination of the Induced magnetic field (about 3°, NNE-SSW direction). This behaviour could suggest the presence of a ferromagnetic causative source having an anthropic origin.

The distribution of analytic signal (Fig. 2c) identifies a main N–S magnetic structure which is clearly divided in two main portions with an asymmetric elongation: the longer and smaller portions of the structure occur at southern and northern edges of the study area, respectively. The two segments seem both placed between 700 and 1500 m b.s.l. with an average depth of the centroids about 1200 m (max. depth 1700 m); the southernmost edge of the structure seems to rise upward in shallower position (minimum depth 500 m. b.s.l). The north-eastern cluster of

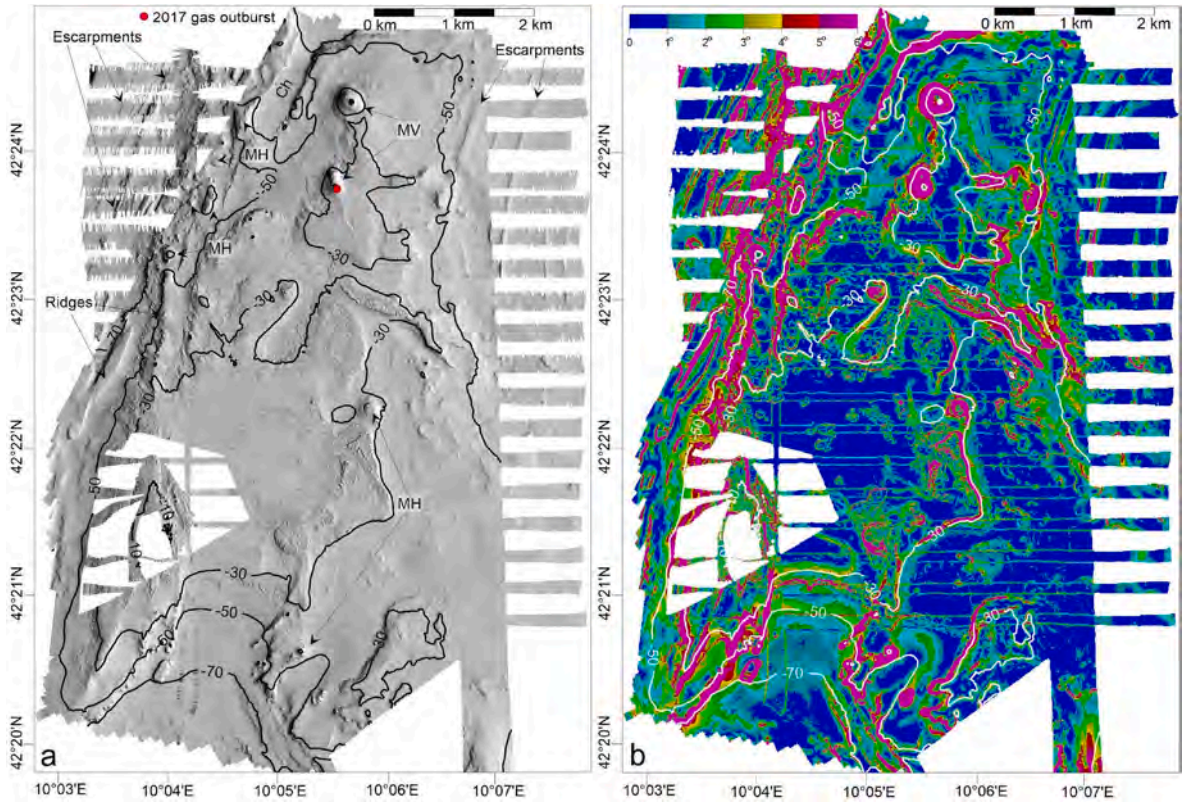

Fig. 3. (**a**) Shaded relief map (artificial sunlight from E) and isobaths (equidistance 20 m) of the study area, with the indication of the main geomorphic features; MV: mud volcano, MH: morphological high, Ch: channel. (**b**) slope gradients map of the study area.

solutions shows an increasing depth without a clear correlation with analytic signal. These solutions could be associated with a low frequency-low amplitude regional magnetic pattern. The south-eastern magnetic anomaly seems linked to a very shallow source (or a cluster of sources) located at depth <200 m (min. depth 114 m). This can suggest its anthropic origin. Anyway, in this sector, the Euler's deconvolution process was very unstable with a large number of uncertain solutions (many depth values very close to the seafloor). Considering this ambiguity coupled to the undefined nature of this source and the lack of other independent data, our interpretation will be mainly focused on the western sector of the study area.

The peculiar setting of the Scoglio d'Affrica region was quantitatively modelled by inverting the magnetic anomaly field (Fig. 4). This approach permitted to reconstruct the 3D distribution of the magnetic susceptibility of a crustal volume limited between the seafloor and a flat bottom layer placed at about 3 Km of depth. We provided a simple representation of the inverse model highlighting a set of isosurfaces encompassing most of the rock having positive susceptibility (≥0.02 SI). The resulting model highlights the presence of a major N–S elongated body having middle-high susceptibility (>0.05 SI) which extends for the entire length of the area of interest (Fig. 4 and additional views in Fig. S3). This structure seems to be divided in two major branches: a 2.5

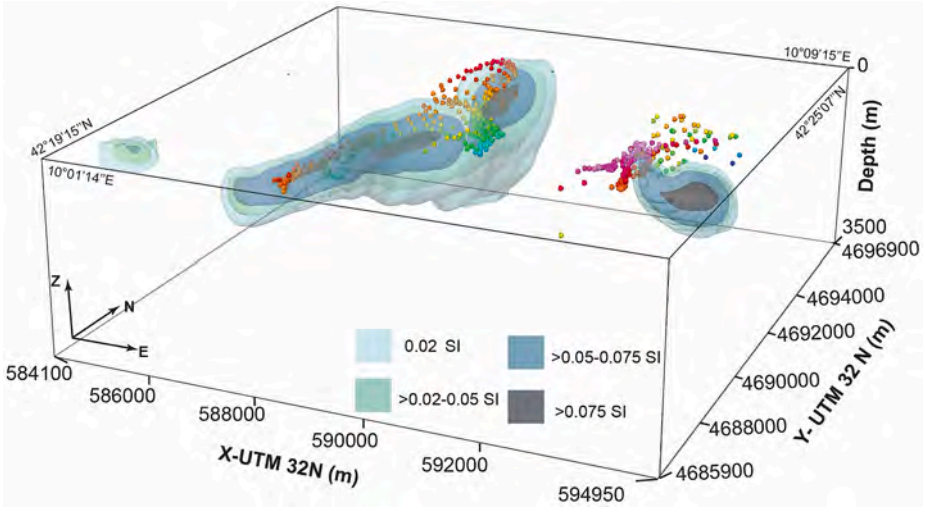

Fig. 4. 3D inverse model of Scoglio d'Affrica region; nested isosurfaces range from 0.02 SI (light blue) to 0.08 SI (dark blue) encompassing most of the source rock volume with magnetic properties. View from South-East. Coloured circles indicate 3D distribution of the Euler's solutions (see Fig. 2c).

km long northern tip which tends to enlarge in volume and gently deepening northward reaching a depth of about 2300 m b.s.l.; the southern branch shows a 7.5 km long, tapered body placed at an average depth of 1500 m. Moving to the inner portion of this elongated body the magnetic susceptibility tends to increase reaching a value of 0.08 SI, which is a value highly compatible with the results obtained by the previous forward model. Depth distribution of the susceptibility structures highlighted in the inverse model matches very well the position of the Euler's solutions (Fig. 2c).

4.3. Seismic data

The interpretation of the six seismic lines (single and multichannel) was mainly performed using the stratigraphic sequence derived from Martina-1 and Mimosa-1 wells (Fig. 1b). The well logs have been used as primary constraint to map (in depth position) the ophiolitic deposits/turbiditic sequence along the different seismic lines.

The two explorative drillings, located at the top of the EPR (Fig. 1b), detect rocks from Eocene (unit SUB1), Oligocene (unit SUB2) and Early Miocene (unit LIT0) without any significant records about Middle-Late Miocene sedimentary events; very thin layers of Pleistocene age are also detected at the top of the two wells.

The Late Miocene to Pleistocene sedimentary sequence forming the EPR is well described in the sparker (Fig. 5) and CROP profiles (Fig. 6). Westward, a well-stratified and mainly not-deformed sedimentary unit, interpreted as Pliocene-Quaternary sequence, thickens up to about 990 m within the Corsica Basin (Fig. 5), assuming an average seismic velocity of 2000 m/s. This unit reaches a similar thickness in an N–S oriented inner basin to the east.

The entire Corsica-Tuscany sector is generally deformed by Tortonian-Messinian extensional tectonics (Pascucci et al., 1999; Moeller et al., 2013; Loreto et al., 2021) , as confirmed by Early Messinian syn-rift deposits (base of Pliocene, in dark green line, Figs. 5 and 6). On the western side of EPR, the Corsica basin, filled by Eocene-Quaternary sediments (Figs. 5 and 6a), is bounded by a main extensional W-dipping faults related to the opening of the basin (Pascucci, 2005). On the eastern and northern side, sediments are dislocated by E and W-dipping major listric and minor normal faults (Figs. 5 and 6b), forming graben or half-graben systems, also shown in Bartole (1995). Such normal faults allowed the formation of Pianosa and Montecristo basins having maximum depths of 280 m and 450 m, respectively (Fig. 6a).

The extensional system deforms the Eocene sediments previously uplifted and folded by a compressional tectonic, linked to the Ligurian-Provençal phase (Principi and Treves, 1984; Mauffret and Contrucci, 1999; Brunet et al., 2000), as also inferred by the folded deep sediments observed within seismic images (Fig. 6). Notably, in the easternmost part of the sparker profile BCO-02 (see CDPs 0–5000 in Fig. 5a), two gentle folds deform the entire Miocene to Pliocene sedimentary sequence, indicating a potential recent shortening phase with W-vergence. Episodes of Late Miocene compressive pulses are also observed in the westernmost portion of Tuscan shelf (Buttinelli et al., 2024) and in the inner sector of the northern Apennine chain (Bonini et al., 2014).

Additional oil and gas exploration seismic lines T12 and T9 (Fig. 7, Fig. S2, respectively; location in Fig. 1a) have been also studied in order to add further stratigraphic details of northern and southern portions of EPR. T12 lines (Fig. 7) runs in E-W direction very close to the Martina-1 well (projected). In the western side, the Eocene-Early Miocene sedimentary sequence tends to be thicker in the centre of the Corsica Basin, becoming instead thinner on the eastern side. Eastward, the sediments are deformed by major E-verging detachment faults that shifted down the bottom of the Early Miocene unit at the same level of the bottom of the Oligocene (see shot-points 420–480, Fig. 7). The seismic line T9 (Fig. S2) highlights a similar structural pattern with a clear rising up of Oligocene unit (probably also Eocene) in proximity of EPR (shot point 400). East of the structural high two east-verging normal faults displace the base of Early Miocene unit. Pliocene deposits seem not be recognized along this profile.

5. Discussion

The magnetic anomaly field of Scoglio d'Affrica region presents a very distinct pattern, notable intriguing given that the EPR is predominantly composed of a more than 3-km thick Eocene-Miocene siliciclastic sequence overlying a crystalline basement (Cornamusini et al., 2002). All these sedimentary units are featured by a very low magnetic

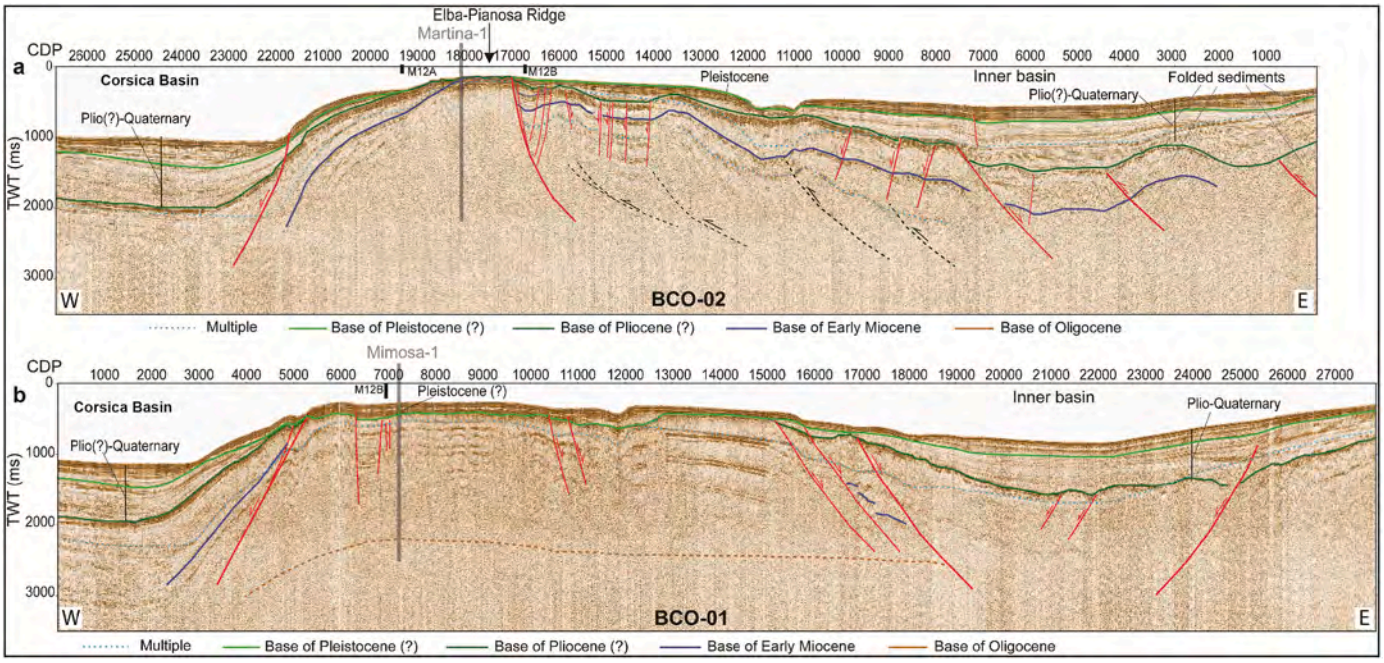

Fig. 5. High resolution sparker profiles BCO-02 (**a**) and BCO-01 (**b**) with superimposition of the interpretative line-drawing (tracks of the profiles are reported in Fig. 1a); position explorative wells are projected and graphically represented with grey bars. Intersection with other seismic profiles is marked with small black bars.

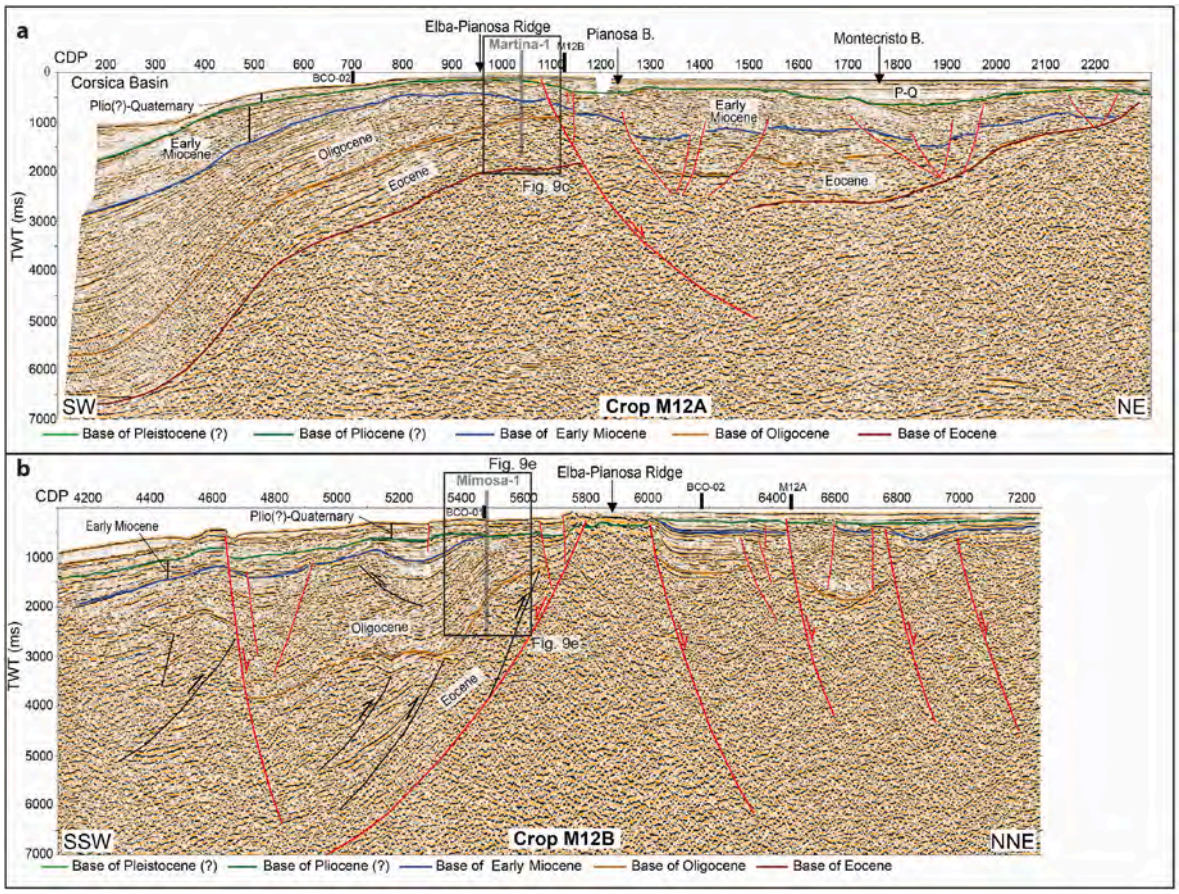

Fig. 6. Interpretation of the multichannel seismic profiles M12A (**a**) and M12B (**b**) from CROP database (CROsta Profonda; www.crop.cnr.it); tracks of seismic lines are shown in Fig. 1a. Black rectangles identify the inset of Fig. 9e.

susceptibility. The inverse model of magnetic anomaly field (Fig. 4, Fig. S3) reveals the presence of a N–S elongated high magnetic susceptibility body formed by the overlapping of two main elements: i) a deeper northern branch having a N–S extension of about 2.5 km; ii) a central-southern magnetic source extending for about 7.5 km.

The interpretation of inverse model is not unique; in fact, the same susceptibility distribution could be associate with rock-sources of different nature, specifically either: a) Fe-rich intrusive magmatic body or b) high grade serpentinite/ophiolite deposits.

We can dismiss the first hypothesis for several reasons: a) a potential magmatic intrusion should be linked to the neighbouring monzogranite rocks forming Montecristo Island (Innocenti et al., 1997), that are characterized by very low magnetic susceptibility (i.e. Vercelli Smt; Cocchi et al., 2016); b) the magnetic body extends along a flat layer at depth of 2000/2500 m without any vertical root, excluding the possibility of a classic deep magmatic plumbing system; c) magmatic intrusions typical exhibit seismic facies characterized by highly discontinuous and reflective horizons forming chaotic signature (e.g. Firetto Carlino et al., 2019; Loreto et al., 2021). No evidence of these seismic features has been identified in the study area (Figs. 5, Fig. 6, Fig. 7).

On the other hand, we argue that the observed magnetic anomaly pattern could be more readily associated with ophiolite/serpentinite deposits commonly characterized by medium to high magnetic susceptibility values (i.e. Maffione et al., 2014 and references therein). This hypothesis is corroborated especially considering that some layers of this material were intersected by both Mimosa-1 and Martina-1 wells.

To validate this interpretation, we performed a 2.5D magnetic forward model along the W-E profile (track A-A' in Fig. 2b), which intersects orthogonally the N–S elongated magnetic body (Fig. 8).

This cross section shows a primary bedrock composed by Mesozoic limestones with low susceptibility (from 0.005 to 0.01 SI) overlaid by approximately 500 m thick of marine sediments showing almost null magnetic signature (0.005 SI). The susceptibility values of these sedimentary layers come from the literature (Telford et al., 1990). The thickness of these different layers was extrapolated from the Martina-1 well (Fig. 1b and reported as inset of Fig. 8), located a few km north to the study area. This well displays a continuous stratigraphy without any record of duplication of the succession (thrust overcoming) as instead observed in the Mimosa-1 well-log (Cornamusini et al., 2002).

The best fitting (misfit error of 1.551 nT) between observed and computed magnetic profiles was achieved by introducing a high susceptibility body that extends in depth from 1760 m to 2200 m, with its centroid situated around 1900 m. In light of the Martina-1 well log, we attribute the causative source to the presence of ophiolite/high-grade serpentinized clasts and blocks embedded in turbiditic-like deposits, originating from the Alpine Corsica region (Cornamusini and Pascucci, 2014). Consequently, our model was constrained using a susceptibility value for the recovered ophiolitic deposit equal to those of Corsica-West Alpine serpentinite rocks (0.08–0.09 SI; Bonnemains et al., 2016).

The geophysical model reveals that ophiolitic deposits of Scoglio d'Affrica are emplaced at a shallower depth (about 200 m) than the sedimentary sequence of the Martina-1 well (average meter 2100 m). This discrepancy could simply be attributed to the non-uniform sedimentary input across the entire EPR. Considering the sedimentary nature of these deposits, it is plausible to assume that their depth location and thickness can vary from site to site along the EPR. In these terms, clear differences are evident when transitioning from the southern Mimosa-1 wells to the northern Martina-1 site.

It is noteworthy that the forward model may not entirely represent

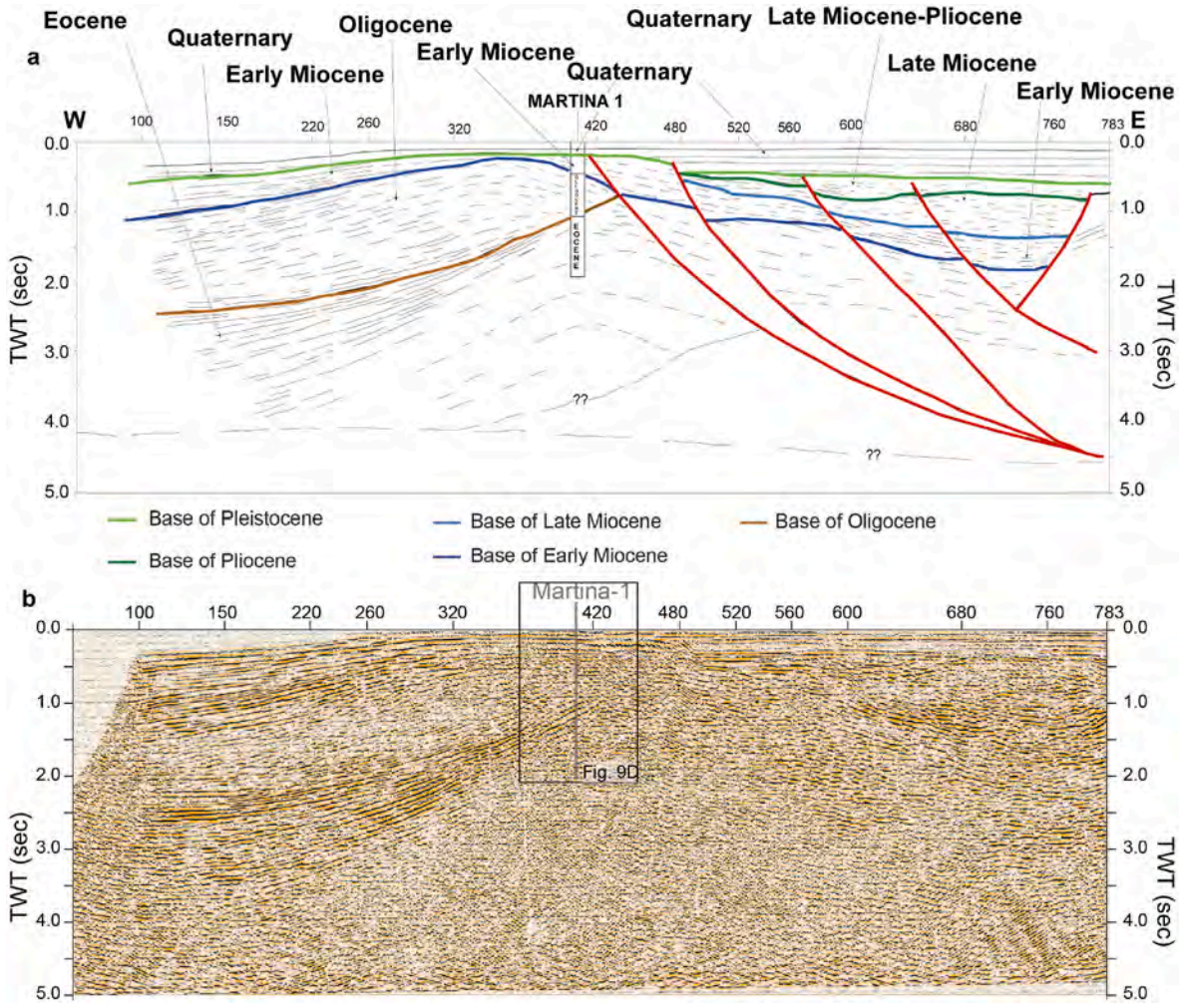

Fig. 7. (**a**) Line drawing relative to the seismic profile T12, crossing the Martina-1 well (projected). Location is shown in Fig. 1a. (**b**) The uninterpreted migrated T12 seismic profile; rectangle identified the inset reported in Fig. 9d.

the real distribution of the diverse lithologies constituting the whole thickness (2500 m) of the crustal section. This methodology does not facilitate the identification of small-scale magnetic susceptibility variations (such as fine-sized clastic material diluted in the stratigraphic column) but tends to average magnetic properties over macro sectors of the cross-section. As a consequence, slight discrepancies in terms of depth and vertical extension of the modelled bodies compared to the real ones may occur.

The latest outcomes of our magnetic modelling and seismo-stratigraphic analysis offer a comprehensive depiction of the tectonic setting in the EPR, uncovering the occurrence of shallow ophiolitic deposits within the Eocene siliciclastic unit, already punctually identified by explorative wells. Significantly, these deposits exhibit a distinctive alignment primarily along the western margin of the EPR. This can be attributed to i) the preferential deposition of coarse–gravel turbiditic material linked to flows originating from the west and ii) variation in rates and deformation styles passing from external to internal margin of the EPR. In this context, the western EPR margin exhibits significant compressional deformation encompassing the entire sedimentary sequence, ranging from Pliocene to Eocene. Progressing eastward, into the inner sections of the Pianosa and Montecristo basins, east-dipping normal faults induce a downward shift in the Eocene unit and its associated ophiolitic deposits. This structural pattern is well depicted by the isochrones map (Fig. 9a) related to the top of Eocene strata, where ophiolite clasts are embedded. These units swiftly ascend towards the EPR structural high, forming a circular minimum of approximately 0.5 s (TWT) in proximity to the Scoglio d'Affrica region (Fig. 9a), where they are abruptly interrupted by a set of east-verging listric faults (Figs. 6a and 7, Fig. S2). The asymmetric tectonic and sedimentary style evident across the EPR results in a peculiar pattern magnetic anomaly field characterized by a high-intensity positive anomalies along the western margin which gradually vanishes towards the eastern portion (Fig. 2a, Fig. S1).

The stratigraphic sequences retrieved from explorative wells also highlight that the ophiolites deposits are placed within the Eocene strata, about 1.5–2 km below the gas enriched sediments predominantly found within the Oligocene succession, as evidenced by the Mimosa-1 well. Additionally, minute gas-bearing layers are discernible within the Miocene units, as observed in the upper segment of the Marina-1 log (at depth of 500/550 m; see Videpi repository).

Only Martina-1 well detects Miocene units where very tiny gas–bearing layers are also present (at depth of 500/550 m). To better understand the relationship between ophiolites deposits and gas-enriched sediments, we projected these levels on the M12a-b seismic lines and on the T12 multi-channel seismic profile (Fig. 9c–e). These results prompt intriguing questions about a potential correlation between the presence of ophiolitic deposits, the observed mud volcanism and methane-enriched gas up-flow in the Scoglio d'Affrica region. Nonetheless, as indicated by Saroni et al. (2020), the gas emissions in the proximity of the mud volcano at Scoglio d'Affrica are primarily composed of CH_4 (95–96.8 vol%), exhibiting an isotopic signature consistent with a thermogenic origin. While we cannot definitively

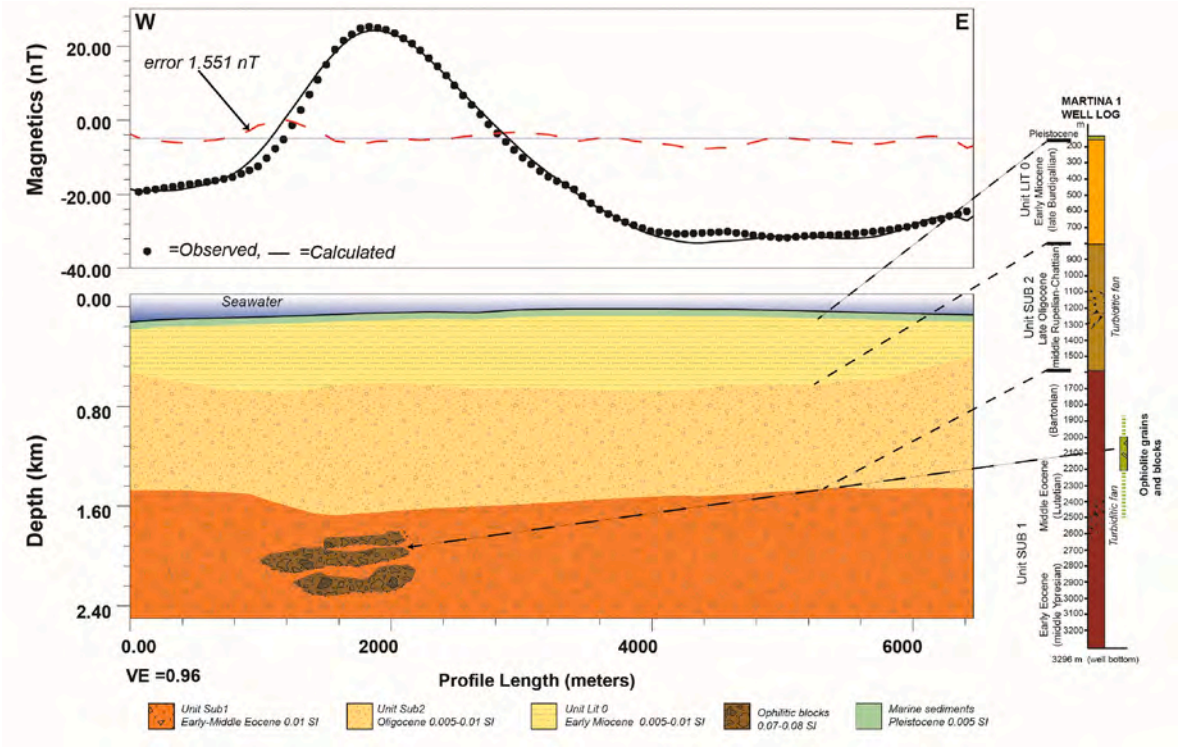

Fig. 8. 2.5D magnetic forward model of Scoglio d'Affrica offshore area. Observed magnetic profile was obtained sampling every 65 m the gridded magnetic anomaly field along the A-A′ profile (track shown in Fig. 2b). On the right side we report the stratigraphic sequence of Martina-1 well (simplified from Cornamusini and Pascucci, 2014).

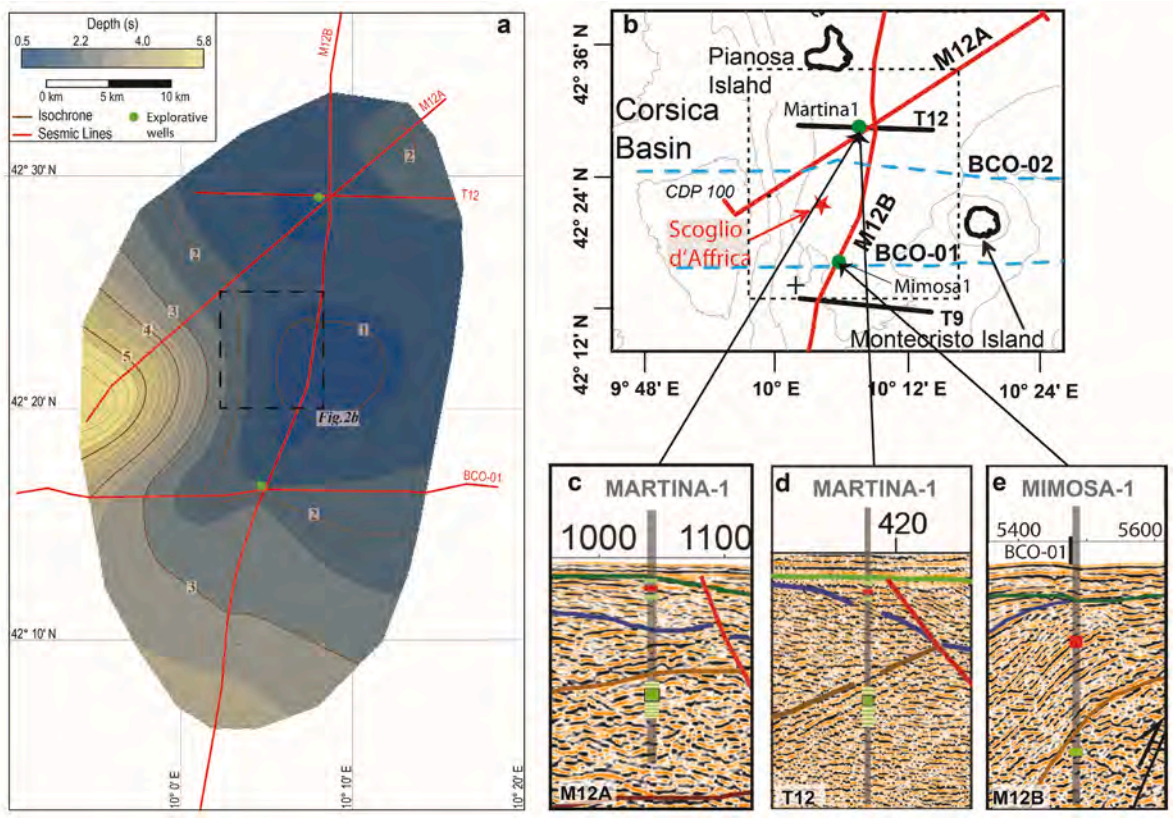

Fig. 9. (**a**) Contour map of the top of the Eocene seismic horizon (time-derived) reconstructed combining high resolution sparker (BCO-01, Fig. 5b), CROP seismic profiles (Fig. 6) and T12 line (Fig. 7). (**b**) Distribution of seismic lines used for the compilation of the top of Eocene map (a); (**c-e**) Inset of seismic lines (Figs. 5, Fig. 6, Fig. 7) with the position of ophiolites (green) and gas-enriched (red) deposits projected from Martina-1 and Mimosa-1 wells.

establish a relationship between gas emissions/mud volcanism and the presence of 10-km-long shallow ophiolitic deposits, this latter structural/sedimentary element aligns remarkably well with the geodynamic scenario of this sector of the Tyrrhenian Sea.

During the Eocene, the EPR-Corsica basin evolved into a thrust-top system (Mauffret et al., 1999), resulting in the deposition of approximately 3 km of siliciclastic material, primarily associated with turbiditic-like fan systems fed by the eastern Alpine-Corsica region (Fig. 10). In this context, the aggregates of ophiolitic/serpentinitic material (block and clasts) can be interpreted as olitostromes within Eocene siliciclastic unit. These are related to the block and/or mass slides originated from peripheral highs and accumulated in intra-wedge or piggy-back basins inverted during the Oligocene (Cornamusini et al., 2002). The sedimentary infilling of intra-wedge basins persisted also during the Oligocene (see Figs. 5, Fig. 6, Fig. 7). Contextually, in this period, the EPR area experienced the effects of a strike-slip fault zone (Turco et al., 2012), leading to the deformation of the existing detrital deposits. This is evident in the Mimosa-1 well-log, which demonstrates a doubled sedimentary sequence (Fig. 1b). Since the Miocene, the extension phase has been relevant, giving rise to a series of normal faults that

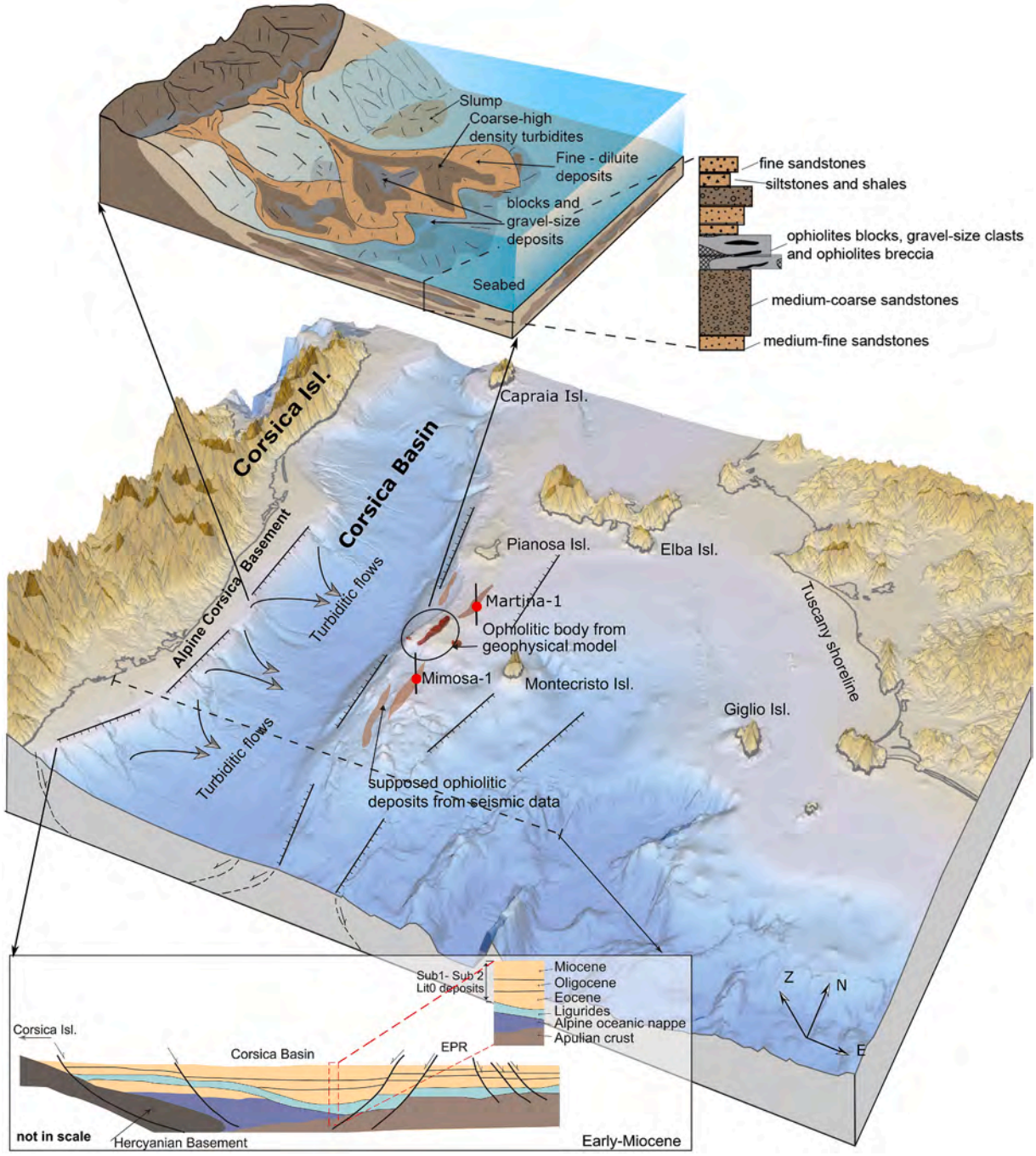

Fig. 10. 3D sketch of the Corsica Basin-Tuscany Archipelago, with location of ophiolitic deposit depicted by magnetic model. Additionally, ophiolitic bodies identified along different seismic lines and well logs (red dots) are also reported as simple cartoons (not in scale). On the upper side, we present a schematic illustration of a turbiditic system (high and low density); idealized vertical stacking pattern has been derived and simplified from Eocene sequence of Martina-1 well. Cross-section (lower inset) represents the tectonic/structural setting of the Corsica-EPR transect during the Early Miocene (simplified from Cornamusini and Pascucci, 2014).

shaped the EPR region and led to the formation of structural highs. In the current geodynamical context, the Scoglio d'Affrica forms a segment of a larger morphologic high, bordered by high-angle normal faults that were active during the post-Burdigalian extensional stage (Cornamusini et al., 2002) (Figs. 5, Fig. 6, Fig. 7, Fig. 10). The crustal fragmentation has involved very shallow structural layer promoting the emplacement of mud volcanoes and fluid seeps; they typically manifest at the crests of the fault system, whether normal or back thrust where secondary brittle features associated with fold growth serves as primary conduits for fluid migration (Bonini, 2012). The gas emissions along EPR may be attributed to the reactivation of local shallow normal fault systems, which acted as primary pathways for the upwelling of CH_4-bearing fluids originating from the nearby Eocene-Oligocene intra-wedge sedimentary basins.

6. Conclusion

A comprehensive interpretative crustal model of Scoglio d'Affrica has been developed, integrating magnetic, morphologic, seismic, as well as stratigraphic (well-log) data. The Scoglio d'Affrica is an emerged segment of the southern EPR and is notable for widespread fluid seepage, featuring multiple active shallow-water mud volcanoes, as testified by the recent explosive gas outburst occurred in 2017 a few km far from the islet.

The quantitative interpretation of magnetic data involved the combination of direct and inverse magnetic models constrained by stratigraphic records obtained from different seismic profiles and two explorative wells. The latest findings outline the presence of an N–S elongated body placed about 2000 m b.s.l, exhibiting high magnetic susceptibility. Considering the stratigraphic succession of the area, this body is interpreted as deposit of clasts and blocks of ophiolites/serpentinites placed which are originated from the disruption of Alpine Corsica basement. This sedimentary unit can be interpreted as allochthonous, indicating a distinct provenance in contrast to the internal Ligurian ophiolites units that are partly exposed in proximity of the nearby Elba Island.

Seismo-stratigraphic analysis additionally depicts that the ophiolitic materials are positioned below the gas-enriched layers (mainly found within Oligocene successions) in proximity to normal faults flanking the EPR structural high. The coexistence of shallow ophiolite-like deposits just beneath a mud volcano, affected by moderate gas leakages, can sparks speculative yet stimulating discussions about the causes of the recent episodic gas burst in the study area. Nonetheless, a definitive answer to this intriguing scientific question necessitates additional data.

The outcomes derived from the magnetic model introduce novel interpretative elements shedding light on the crustal setting of the Scoglio d'Affrica region. Here we observe a convergence of multiphase tectonic deformation, the presence of shallow ophiolitic-like deposits and mud volcanism with active gas exhalations. All these features provide a fascinating subject for exploration and invites further investigation into the complex geological processes shaping the Scoglio d'Affrica region.

Funding

Funding to VP is from NBFC to University of Sassari, funded by the Italian Ministry of University and Research, PNRR, Missione 4 Componente 2, "Dalla ricerca all'impresa", Investimento 1.4, Project CN00000033.

Funding to LC is from INGV - Pianeta Dinamico 2020–2022 project.

CRediT authorship contribution statement

Luca Cocchi: Writing – original draft, Investigation, Data curation, Conceptualization. **Filippo Muccini:** Writing – original draft, Methodology, Data curation. **Daniele Casalbore:** Writing – original draft, Validation, Methodology, Data curation. **Francesco Latino Chiocci:** Writing – original draft, Validation, Supervision. **Maria Filomena Loreto:** Writing – original draft, Validation, Formal analysis. **Camilla Palmiotto:** Visualization, Validation, Methodology. **Vincenzo Pascucci:** Visualization, Validation, Supervision. **Roberta Ivaldi:** Supervision, Resources. **Gilberto Saccorotti:** Writing – original draft, Supervision, Resources.

Declaration of competing interest

The authors declare that they have no known competing financial interests or personal relationships that could have appeared to influence the work reported in this paper.

Data availability

Data will be made available on request.

Acknowledgements

The authors are grateful to the Captain, officers and the crew of R/V Aretusa of Italian Navy for their collaboration during the oceanographic cruise. Dr. Valentina Ferrante is sincerely acknowledged for her support to the migration processing of the multichannel CROP seismic lines M12A and M12B (CROsta Profonda; http://www.crop.cnr.it/). Seismic data were interpreted using the Kingdom Suite software, freely available in the frame of IHS University Grant Program. Some figures were prepared using GMT (Wessel and Smith, 1998). Authors would like to thank the Section Editor Prof. Thiago Alves, Prof. Marco Antonellini and an anonymous reviewer for all their thorough comments and reviews that improved the quality of the manuscript.

Appendix A. Supplementary data

Supplementary data to this article can be found online at https://doi.org/10.1016/j.marpetgeo.2024.106847.

References

Alken, P., Thébault, E., Beggan, C.D., Amit, H., Aubert, J., Baerenzung, J., Bondar, T.N., Brown, W.J., Califf, S., Chambodut, A., Chulliat, A., Cox, G.A., Finlay, C.C., Fournier, A., Gillet, N., Grayver, A., Hammer, M.D., Holschneider, M., Huder, L., Hulot, G., Jager, T., Kloss, C., Korte, M., Kuang, W., Kuvshinov, A., Langlais, B., Léger, J.-M., Lesur, V., Livermore, P.W., Lowes, F.J., Macmillan, S., Magnes, W., Mandea, M., Marsal, S., Matzka, J., Metman, M.C., Minami, T., Morschhauser, A., Mound, J.E., Nair, M., Nakano, S., Olsen, N., Pavón-Carrasco, F.J., Petrov, V.G., Ropp, G., Rother, M., Sabaka, T.J., Sanchez, S., Saturnino, D., Schnepf, N.R., Shen, X., Stolle, C., Tangborn, A., Tøffner-Clausen, L., Toh, H., Torta, J.M., Varner, J., Vervelidou, F., Vigneron, P., Wardinski, I., Wicht, J., Woods, A., Yang, Y., Zeren, Z., Zhou, B., 2021. International geomagnetic reference field: the thirteenth generation. Earth Planets Space 73, 49. https://doi.org/10.1186/s40623-020-01288-x.

Baranov, V., Naudy, H., 1964. Numerical Calculation of the formula of reduction to the magnetic pole. Geophysics 29, 67–79. https://doi.org/10.1190/1.1439334.

Barber, A.J., Tjokrosapoetro, S., Charlton, T.R., 1986. Mud volcanoes, shale diapirs, wrench faults, and melanges in accretionary complexes, eastern Indonesia. Am. Assoc.Pet. Geol. Bull. 70, 1729–1741. https://doi.org/10.1306/94886CA9-1704-11D7-8645000102C1865D.

Barletta, S., Del Bono, G.L., Salvati, L., 1969. Nota preliminare sui lavori geomorfologici e geominerari subacquei effettuati dal Servizio Geologico d'Italia dal 1964 al 1969. Boll. Serv. Geol. Ital. CX, 83–89.

Bartole, R., 1995. The North Tyrrhenian-Northern Apennines post-collisional system: constraints for a geodynamic model. Terra Nova 7, 7–30. https://doi.org/10.1111/j.1365-3121.1995.tb00664.x.

Bonini, M., 2007. Interrelations of mud volcanism, fluid venting, and thrust-anticline folding: examples from the external northern Apennines (Emilia-Romagna, Italy). J. Geophys. Res. 112, B08413 https://doi.org/10.1029/2006JB004859.

Bonini, M., 2012. Mud volcanoes: indicators of stress orientation and tectonic controls. Earth Sci. Rev. 115, 121–152. https://doi.org/10.1016/j.earscirev.2012.09.002.

Bonini, M., Sani, F., Stucchi, E.M., Moratti, G., Benvenuti, M., Menanno, G., Tanini, C., 2014. Late Miocene shortening of the northern apennines back-arc. J. Geodyn. 74, 1–31. https://doi.org/10.1016/j.jog.2013.11.002.

Bonnemains, D., Carlut, J., Escartín, J., Mével, C., Andreani, M., Debret, B., 2016. Magnetic signatures of serpentinization at ophiolite complexes: magnetism of

ophiolite serpentinites. G-cubed 17, 2969–2986. https://doi.org/10.1002/2016GC006321.
Bossio, A., Cornamusini, G., Ferrandini, J., Ferrandini, M., Foresi, L., Mazzanti, R., Mazzei, R., Salvatorini, G., 2000. L'evoluzione sedimentaria neogenica dell'area tirrenica settentrionale (Toscana Marittima, Isola di Pianosa, Bacino di Aléria). Presented at the Proceedings of the Environment et Identité en Mediterranée Congress, Corte, France, France.
Brown, K.M., 1990. The nature and hydrogeologic significance of mud diapirs and diatremes for accretionary systems. J. Geophys. Res. 95, 8969. https://doi.org/10.1029/JB095iB06p08969.
Brunet, C., Monié, P., Jolivet, L., Cadet, J.-P., 2000. Migration of compression and extension in the Tyrrhenian Sea, insights from 40Ar/39Ar ages on micas along a transect from Corsica to Tuscany. Tectonophysics 321, 127–155. https://doi.org/10.1016/S0040-1951(00)00067-6.
Buttinelli, M., Mazzarini, F., Musumeci, G., Maffucci, R., Maesano, F.E., Cavirani, I., Diviacco, P., 2024. Tectonic-sedimentary evolution of the tuscan shelf (Italy): seismic-stratigraphic/structural analysis of neogenic succession in the Tyrrhenian Sea between Elba island and Monte argentario promontory. Tectonophysics 873, 230211. https://doi.org/10.1016/j.tecto.2024.230211.
Caratori Tontini, F., Stefanelli, P., Giori, I., Faggioni, O., Carmisciano, C., 2004. The revised aeromagnetic anomaly map of Italy. Ann. Geophys. 47, 3. https://doi.org/10.4401/ag-3358.
Carminati, E., Doglioni, C., 2012. Alps vs. Apennines: the paradigm of a tectonically asymmetric Earth. Earth Sci. Rev. 112, 67–96. https://doi.org/10.1016/j.earscirev.2012.02.004.
Casalbore, D., Ingrassia, M., Pierdomenico, M., Beaubien, S.E., Martorelli, E., Bigi, S., Ivaldi, R., DeMarte, M., Chiocci, F.L., 2020. Morpho-acoustic characterization of a shallow-water mud volcano offshore Scoglio d'Affrica (Northern Tyrrhenian Sea) responsible for a violent gas outburst in 2017. Mar. Geol. 428, 106277.
Cocchi, L., Masetti, G., Muccini, F., Carmisciano, C., 2016. Geophysical mapping of Vercelli seamount: implications for Miocene evolution of the Tyrrhenian back arc basin. Geosci. Front. 7, 835–849. https://doi.org/10.1016/j.gsf.2015.06.006.
Cornamusini, G., Lazzarotto, A., Merlini, S., Pascucci, V., 2002. Eocene–miocene evolution of the north Tyrrhenian Sea. Boll. Soc. Geol. Ital. 1, 769–787.
Cornamusini, G., Pascucci, V., 2014. Sedimentation in the northern apennines–corsica tectonic knot (northern Tyrrhenian Sea, central mediterranean): offshore drilling data from the elba–pianosa ridge. Int. J. Earth Sci. 103, 821–842. https://doi.org/10.1007/s00531-014-0998-5.
Del Bono, G.L., Giammarino, S., 1968. Rinvenimento di manifestazioni metanifere nelle Praterie a Posidonie sui fondi marini prospicienti lo «Scoglio d'Africa» nell'Arcipelago Toscano. Atti Ist. Geol. Univ. Genova 6 (1), 11.
Ellis, R.G., MacLeod, I.N., 2013. Constrained voxel inversion using the Cartesian cut cell method. ASEG Ext. Abstr. 2013, 1–4. https://doi.org/10.1071/ASEG2013ab222.
EMODnet Bathymetry Consortium. EMODnet digital bathymetry (DTM 2020). https://doi.org/10.12770/bb6a87dd-e579-4036-abe1-e649cea9881a.
Fabbri, A., Gallignani, P., Zitellini, N., 1981. Geological evolution of the peri-Tyrrhenian sedimentary basins. In: Wezel, F.C. (Ed.), Sedimentary Basins of Mediterranean Margins. Tecnoprint, Bologna, pp. 101–126.
Faccenna, C., Funiciello, F., Giardini, D., Lucente, P., 2001. Episodic back-arc extension during restricted mantle convection in the Central Mediterranean. Earth Planet Sci. Lett. 187, 105–116. https://doi.org/10.1016/S0012-821X(01)00280-1.
Faccenna, C., Mattei, M., Funiciello, R., Jolivet, L., 1997. Styles of back-arc extension in the central mediterranean. Terra Nova 9, 126–130. https://doi.org/10.1046/j.1365-3121.1997.d01-12.x.
Farran, M., 2008. IMAGE2SEGY: una aplicación informática para la conversión de imágenes de perfiles sísmicos a ficheros en formato SEG Y. Geotemas 10, 1215–1218.
Ferrante, V., Rovere, M., Loreto, M.F., 2023. Preservazione del dato sismico: dal "vintage" cartaceo al digitale. Open Access Tecnical Report. CNR-ISMAR. https://doi.org/10.26383/CNR-ISMAR.2023.2.
Ferretti, R., Caccia, M., Coltorti, M., Ivaldi, R., 2021. New approaches for the observation of transient phenomena in critical marine environment. J. Mar. Sci. Eng. 9, 578. https://doi.org/10.3390/jmse9060578.
Finetti, I.R., 2005. CROP Project: Deep Seismic Exploration of the Central Mediterranean and Italy. Elsevier, Amsterdam.
Firetto Carlino, M., Cavallaro, D., Coltelli, M., Cocchi, L., Zgur, F., Patanè, D., 2019. Time and space scattered volcanism of Mt. Etna driven by strike-slip tectonics. Sci. Rep. 9, 12125 https://doi.org/10.1038/s41598-019-48550-1.
FitzGerald, D., Reid, A., McInerney, P., 2004. New discrimination techniques for Euler deconvolution. Comput. Geosci. 30, 461–469. https://doi.org/10.1016/j.cageo.2004.03.006.
Gueguen, E., Doglioni, C., Fernandez, M., 1998. On the post-25 Ma geodynamic evolution of the western Mediterranean. Tectonophysics 298, 259–269. https://doi.org/10.1016/S0040-1951(98)00189-9.
Henry, P., Le Pichon, X., Lallemant, S., Foucher, J., Westbrook, G., Hobart, M., 1990. Mud volcano field seaward of the Barbados Accretionary Complex: a deep-towed side scan sonar survey. J. Geophys. Res. Solid Earth 95, 8917–8929. https://doi.org/10.1029/JB095iB06p08917.
Hedberg, H.D., 1980. Methane generation and petroleum migration. Probl. Pet. Migr. 10, 179–206.
Hedberg, H.D., 1974. Relation of methane generation to undercompacted shales, shale diapirs and mud volcanoes. Bull. Am. Assoc. Pet. Geol. 58, 661–673.
Higgins, G., Saunders, J.B., 1974. Mud volcanoes-their nature and origin. Verhandlungen der Naturforschenden Gesellschaft Basel 84, 101–152.
Ingram, D.M., Causon, D.M., Mingham, C.G., 2003. Developments in Cartesian cut cell methods. Math. Comput. Simulat. 61, 561–572. https://doi.org/10.1016/S0378-4754(02)00107-6.
Innocenti, F., Westerman, D.S., Rocchi, S., Tonarini, S., 1997. The Montecristo monzogranite (Northern Tyrrhenian Sea, Italy): a collisional pluton in an extensional setting. Geol. J. 32, 131–151. https://doi.org/10.1002/(SICI)1099-1034(199706)32:2<131::AID-GJ735>3.0.CO;2-F.
Ivanov, M.K., Limonov, A.F., van Weering, TjC.E., 1996. Comparative characteristics of the black sea and Mediterranean Ridge mud volcanoes. Mar. Geol. 132, 253–271. https://doi.org/10.1016/0025-3227(96)00165-X.
Jolivet, L., Faccenna, C., Goffé, B., Mattei, M., Rossetti, F., Brunet, C., Storti, F., Funiciello, R., Cadet, J.P., d'Agostino, N., Parra, T., 1998. Midcrustal shear zones in postorogenic extension: example from the northern Tyrrhenian Sea. J. Geophys. Res. Solid Earth 103, 12123–12160. https://doi.org/10.1029/97JB03616.
Klein, F., Bach, W., Humphris, S.E., Kahl, W.-A., Jons, N., Moskowitz, B., Berquo, T.S., 2014. Magnetite in seafloor serpentinite–Some like it hot. Geology 42, 135–138. https://doi.org/10.1130/G35068.1.
Kopf, A.J., 2002. Significance of mud volcanism. Rev. Geophys. 40 https://doi.org/10.1029/2000RG000093.
Lagabrielle, Y., Vitale Brovarone, A., Ildefonse, B., 2015. Fossil oceanic core complexes recognized in the blueschist metaophiolites of Western Alps and Corsica. Earth Sci. Rev. 141, 1–26. https://doi.org/10.1016/j.earscirev.2014.11.004.
Limonov, A.F., Woodside, J.M., Cita, M.B., Ivanov, M.K., 1996. The Mediterranean Ridge and related mud diapirism: a background. Mar. Geol. 132, 7–19. https://doi.org/10.1016/0025-3227(96)00150-8.
Loreto, M.F., Zitellini, N., Ranero, C.R., Palmiotto, C., Prada, M., 2021. Extensional tectonics during the Tyrrhenian back-arc basin formation and a new morpho-tectonic map. Basin Res. 33, 138–158. https://doi.org/10.1111/bre.12458.
Maffione, M., Morris, A., Plümper, O., van Hinsbergen, D.J.J., 2014. Magnetic properties of variably serpentinized peridotites and their implication for the evolution of oceanic core complexes. G-cubed 15, 923–944. https://doi.org/10.1002/2013GC004993.
Malavieille, J., Chemenda, A., Larroque, C., 1998. Evolutionary model for Alpine Corsica: mechanism for ophiolite emplacement and exhumation of high-pressure rocks. Terra Nova 10, 317–322. https://doi.org/10.1046/j.1365-3121.1998.00208.x.
Mariani, M., Prato, R., 1988. I Bacini nogenici costieri del margine terrenico: approccio sismo stratigrafico. Mem. Soc. Geol. Ita. 41, 519–531.
Marroni, M., Pandolfi, L., 2003. Deformation history of the ophiolite sequence from the Balagne Nappe, northern Corsica: insights in the tectonic evolution of Alpine Corsica. Geol. J. 38, 67–83. https://doi.org/10.1002/gj.933.
Marroni, M., Meneghini, F., Pandolfi, L., 2010. Anatomy of the Ligure-Piemontese subduction system: evidence from Late Cretaceous–middle Eocene convergent margin deposits in the Northern Apennines, Italy. Int. Geol. Rev. 52, 1160–1192. https://doi.org/10.1080/00206810903545493.
Mascle, J., Mary, F., Praeg, D., Brosolo, L., Camera, L., Ceramicola, S., Dupré, S., 2014. Distribution and geological control of mud volcanoes and other fluid/free gas seepage features in the Mediterranean Sea and nearby Gulf of Cadiz. Geo-Mar. Letters 34, 89–110. https://doi.org/10.1007/s00367-014-0356-4.
Mauffret, A., Contrucci, I., 1999. Crustal structure of the North Tyrrhenian Sea: first result of the multichannel seismic LISA cruise. Geol. Soc. Lond. Spec. Publ. 156, 169–193. https://doi.org/10.1144/GSL.SP.1999.156.01.10.
Mauffret, A., Contrucci, I., Brunet, C., 1999. Structural evolution of the Northern Tyrrhenian Sea from new seismic data. Mar. Petrol. Geol. 16, 381–407. https://doi.org/10.1016/S0264-8172(99)00004-5.
Mazzini, A., Etiope, G., 2017. Mud volcanism: an updated review. Earth Sci. Rev. 168, 81–112. https://doi.org/10.1016/j.earscirev.2017.03.001.
Meister, P., Wiedling, J., Lott, C., Bach, W., Kuhfuß, H., Wegener, G., Böttcher, M.E., Deusner, C., Lichtschlag, A., Bernasconi, S.M., Weber, M., 2018. Anaerobic methane oxidation inducing carbonate precipitation at abiogenic methane seeps in the Tuscan archipelago (Italy). PLoS One 13, e0207305. https://doi.org/10.1371/journal.pone.0207305.
Milkov, A.V., 2000. Worldwide distribution of submarine mud volcanoes and associated gas hydrates. Mar. Geol. 167, 29–42. https://doi.org/10.1016/S0025-3227(00)00022-0.
Milkov, A.V., Sassen, R., Apanasovich, T.V., Dadashev, F.G., 2003. Global gas flux from mud volcanoes: a significant source of fossil methane in the atmosphere and the ocean. Geophys. Res. Lett. 30 https://doi.org/10.1029/2002GL016358.
Moeller, S., Grevemeyer, I., Ranero, C.R., Berndt, C., Klaeschen, D., Sallares, V., Zitellini, N., de Franco, R., 2013. Early-stage rifting of the northern Tyrrhenian Sea Basin: results from a combined wide-angle and multichannel seismic study: rifting Tyrrhenian. G-cubed 14, 3032–3052. https://doi.org/10.1002/ggge.20180.
Molli, G., 2008. Northern Apennine–Corsica orogenic system: an updated overview. Geol. Soc. Lond. Spec. Publ. 298, 413–442. https://doi.org/10.1144/SP298.19.
Motteran, G., Ventura, G., 2005. Aspetti geologici, morfologici e ambientali dello scoglio d'africa (arcipelago toscano): nota preliminare. Atti Soc. Tosc. Sci. nat., Mem., Ser.A 110, 51–60.
Nabighian, M.N., 1984. Toward a three-dimensional automatic interpretation of potential field data via generalized Hilbert transforms: fundamental relations. Geophysics 49, 780–786. https://doi.org/10.1190/1.1441706.
Nuzzo, M., Tomonaga, Y., Schmidt, M., Valadares, V., Faber, E., Piñero, E., Reitz, A., Haeckel, M., Tyroller, L., Godinho, E., Kipfer, R., Terrinha, P.G., Hensen, C., 2019. Formation and migration of hydrocarbons in deeply buried sediments of the Gulf of Cadiz convergent plate boundary - insights from the hydrocarbon and helium isotope geochemistry of mud volcano fluids. Mar. Geol. 410, 56–69. https://doi.org/10.1016/j.margeo.2019.01.005.
Oufi, O., 2002. Magnetic properties of variably serpentinized abyssal peridotites. J. Geophys. Res. 107, 2095. https://doi.org/10.1029/2001JB000549.

Pascucci, V., 2005. The tuscan shelf as imaged by the CROP-m12a line. Boll. Soc. Geol. Ital. 3, 167–178.
Pascucci, V., 2002. Tyrrhenian Sea extension north of the Elba island between Corsica and western Tuscany (Italy). Boll. Soc. Geol. Ital. 1 (Spec. issue), 819–828.
Pascucci, V., Merlini, S., Martini, P., 1999. Seismic stratigraphy of the miocene-pleistocene sedimentary basins of the northern Tyrrhenian Sea and western Tuscany (Italy): sedimentation in the southern subalpine chains. Basin Res 11, 337–356. https://doi.org/10.1046/j.1365-2117.1999.00104.x.
Pettke, T., Bretscher, A., 2022. Fluid-mediated element cycling in subducted oceanic lithosphere: the orogenic serpentinite perspective. Earth Sci. Rev. 225, 103896 https://doi.org/10.1016/j.earscirev.2021.103896.
Praeg, D., Ceramicola, S., Barbieri, R., Unnithan, V., Wardell, N., 2009. Tectonically-driven mud volcanism since the late Pliocene on the Calabrian accretionary prism, central Mediterranean Sea. Mar. Petrol. Geol. 26, 1849–1865. https://doi.org/10.1016/j.marpetgeo.2009.03.008.
Principi, G., Treves, B., 1984. Il sistema corso-appenninico come prisma di accrezione. Riflessi sul problema generale del limite Alpi–Appennini. Mem. Soc. Geol. Ita. 28, 549–576.
Reid, A.B., Allsop, J.M., Granser, H., Millett, A.J., Somerton, I.W., 1990. Magnetic interpretation in three dimensions using Euler deconvolution. Geophysics 55, 80–91. https://doi.org/10.1190/1.1442774.
Rovere, M., Gamberi, F., Mercorella, A., Rashed, H., Gallerani, A., Leidi, E., Marani, M., Funari, V., Pini, G.A., 2014. Venting and seepage systems associated with mud volcanoes and mud diapirs in the southern Tyrrhenian Sea. Mar. Geol. 347, 153–171. https://doi.org/10.1016/j.margeo.2013.11.013.
Rovere, M., Mercorella, A., Gamberi, F., Zgur, F., 2022. Hydrothermal vent complexes control seepage and hydrocarbon release on the overriding plate of the tyrrhenian-ionian subduction system (paola basin). Front. Earth Sci. 10, 852786 https://doi.org/10.3389/feart.2022.852786.
Saroni, A., Sciarra, A., Grassa, F., Eich, A., Weber, M., Lott, C., Ferretti, G., Ivaldi, R., Coltorti, M., 2020. Shallow submarine mud volcano in the northern Tyrrhenian sea, Italy. Appl. Geochem. 122, 104722 https://doi.org/10.1016/j.apgeochem.2020.104722.
Savelli, C., 2000. Subduction-related episodes of K-alkaline magmatism (15 ± 0 . 1 Ma) and geodynamic implications in the north Tyrrhenian Ð central Italy region : a review. J. Geodyn. 30, 575–591.
Sciarra, A., Saroni, A., Etiope, G., Coltorti, M., Mazzarini, F., Lott, C., Grassa, F., Italiano, F., 2019. Shallow submarine seep of abiotic methane from serpentinized peridotite off the Island of Elba, Italy. Appl. Geochem. 100, 1–7. https://doi.org/10.1016/j.apgeochem.2018.10.025.
Scrocca, D., Beggan, C., Innocenti, F., Manetti, P., Mazzotti, A., Bertelli, L., Burbi, L., D'Offizi, S., 2003. CROP Atlas: seismic reflection profiles of the Italian crust. Mem. Descr. Carta. Geol. Ita. 62, 1–193.
Serri, G., Innocenti, F., Manetti, P., 2001. Magmatism from Mesozoic to Present: petrogenesis, time-space distribution and geodynamic implications. In: Vai, G.B., Martini, I.P. (Eds.), Anatomy of an Orogen: the Apennines and Adjacent Mediterranean Basins. Springer, Netherlands, Dordrecht, pp. 77–103. https://doi.org/10.1007/978-94-015-9829-3_8.
Spatola, D., Casalbore, D., Pierdomenico, M., Conti, A., Bigi, S., Ingrassia, M., Ivaldi, R., Demarte, M., Napoli, S., Chiocci, F.L., 2022. Seafloor characterisation of the offshore sector around Scoglio d'Affrica islet (Tuscan Archipelago, northern Tyrrhenian sea). J. Maps 1–10. https://doi.org/10.1080/17445647.2022.2120836.
Speranza, F., Villa, I.M., Sagnotti, L., Florindo, F., Cosentino, D., Cipollari, P., Mattei, M., 2002. Age of the corsica–sardinia rotation and liguro–provençal basin spreading: new paleomagnetic and Ar/Ar evidence. Tectonophysics 347, 231–251. https://doi.org/10.1016/S0040-1951(02)00031-8.
Talwani, M., Heirtzler, J.R., 1964. Computation of magnetic anomalies caused by two-dimensional bodies of arbitrary shape. In: Parks, G.A. (Ed.), Computers in the Mineral Industries (Part 1). Stanford University Publication Geological Science, Stanford, pp. 464–480.
Telford, W.M., Geldart, L.P., Sheriff, R.E., 1990. Applied Geophysics, second ed. Cambridge University Press. https://doi.org/10.1017/CBO9781139167932.
Thompson, D.T., 1982. EULDPH: a new technique for making computer-assisted depth estimates from magnetic data. Geophysics 47, 31–37. https://doi.org/10.1190/1.1441278.
Toft, P.B., Arkani-Hamed, J., Haggerty, S.E., 1990. The effects of serpentinization on density and magnetic susceptibility: a petrophysical model. Phys. Earth Planet. In. 65, 137–157. https://doi.org/10.1016/0031-9201(90)90082-9.
Turco, E., Macchiavelli, C., Mazzoli, S., Schettino, A., Pierantoni, P.P., 2012. Kinematic evolution of Alpine Corsica in the framework of Mediterranean mountain belts. Tectonophysics 579, 193–206. https://doi.org/10.1016/j.tecto.2012.05.010.
Wessel, P., Smith, W.H.F., 1998. New, improved version of generic mapping tools released. Eos Trans. Am. Geophys. Union 79, 579. https://doi.org/10.1029/98EO00426, 579.
Won, I.J., Bevis, M., 1987. Computing the gravitational and magnetic anomalies due to a polygon: algorithms and Fortran subroutines. Geophysics 52, 232–238. https://doi.org/10.1190/1.1442298.
Zoporowski, A., Miller, S.A., 2009. Modelling eruption cycles and decay of mud volcanoes. Mar. Petrol. Geol. 26, 1879–1887. https://doi.org/10.1016/j.marpetgeo.2009.03.003.